Computers, Materials & Continua

Tech Science Press

https://doi.org/10.32604/cmc.2026.075679

ARTICLE

Fixed-Time Bipartite Formation of Multi-Agent Systems Using Dynamic Event-Triggered Scheme

Longquan Ma[1], Huarong Zhao[1,*], Liqin Zhou[1], Linbo Xie[1,*] and Hongnian Yu[2]

[1]Engineering Research Center of Internet of Things Applications Ministry of Education, Jiangnan University, Wuxi, China
[2]School of Computing, Engineering and the Built Environment, Edinburgh Napier University, Edinburgh, UK

*Corresponding Authors: Huarong Zhao. Email: hrzhao@jiangnan.edu.cn; Linbo Xie. Email: xie_linbo@jiangnan.edu.cn

Received: 06 November 2025; Accepted: 10 February 2026; Published: 09 April 2026

ABSTRACT: This paper studies a sampling-based dynamic event-triggered fixed-time bipartite formation algorithm for a class of continuous-time multi-agent systems with communication constraints. First, a periodic sampling mechanism is designed to reduce the system's communication frequency. Then, a dynamic event-triggered control algorithm based on auxiliary variables is developed for sampled-data systems to further reduce the system's triggering frequency. Next, to enhance the convergence speed of the dynamic event-triggered control method, a dynamic event-triggered fixed-time bipartite formation control scheme is investigated. Finally, using Lyapunov stability theory, signed graph theory, and relevant inequalities, a rigorous theoretical proof of the stability of the proposed control protocol is provided, and the algorithm's effectiveness is verified through simulation experiments.

KEYWORDS: Sampled-data; dynamic event-triggered; fixed-time bipartite formation; multi-agent systems

1 Introduction

Due to their flexibility and scalability, multi-agent systems have been widely applied across fields such as spacecraft attitude coordination [1,2], smart grids [3,4], and intelligent transportation [5,6]. Formation control [7–10] is a fundamental problem in the coordination of multi-agent systems, aiming to design distributed control protocols that enable multiple agents to form a desired geometric shape to accomplish complex tasks in challenging environments, such as limited communication bandwidth [11], unknown disturbances [12], and cyber-attacks [13]. Convergence rate is an important performance metric in formation control and remains a topic of active research. In [14–16], asymptotic convergence algorithms were proposed, while in [17–19], finite-time convergence algorithms were presented. Among these, finite-time algorithms converge faster than asymptotic ones. However, the upper bound of the convergence time for finite-time convergence algorithms depends on the system's initial state. To address the upper bound on convergence time in finite-time consensus algorithms, researchers have begun studying fixed-time convergence algorithms [20]. In [21], a fixed-time formation control algorithm for heterogeneous multi-agent systems with disturbances was proposed. In [22], an adaptive optimal fixed-time output feedback formation algorithm for time-varying scenarios was introduced. In [23], a fixed-time formation control algorithm for uncertain nonlinear multi-agent systems with actuator faults was proposed. In addition, some scholars further developed prescribed-time control approaches [24–26]. Although research on fixed-time formation control algorithms exists, these studies primarily focus on cooperative relationships among

agents. Therefore, further research on the competitive relationships among multi-agent systems and on implementing fixed-time formation control for such systems is a meaningful endeavor.

In nature, agents exhibit both cooperative and competitive relationships, as seen in wolf pack hunting. Addressing the cooperation and competition in multi-agent systems, reference [27] first introduced the concept of bipartite consensus. In recent years, researchers have made significant progress in studying bipartite formation in multi-agent systems. In [28], a bipartite formation algorithm for second-order nonlinear multi-agent systems with hybrid pulses was proposed. In [29], a bipartite time-varying formation algorithm for nonlinear multi-agent systems based on disturbance observers was developed. In [30], a fixed-time bipartite time-varying formation tracking algorithm for networked Euler-Lagrange systems was presented. It is noted that although numerous studies have examined bipartite formation control algorithms, few have addressed communication constraints in bipartite formation control for multi-agent systems. Compared with standard consensus problems, bipartite formation issues are more complex because they involve antagonistic relationships and negative weights, which necessitate greater communication and computational resources. Therefore, the main motivation of this paper is to design a fixed-time bipartite formation control algorithm that further reduces communication energy consumption.

In practical applications, continuous controller updates can waste significant communication resources and increase wear on actuators. To overcome these drawbacks, researchers have proposed event-triggered control mechanisms, in which the controller is updated only when event-triggered conditions are met [31,32]. In [33], a data-driven event-triggered bipartite formation control method was designed for nonlinear multi-agent systems with unknown dynamics. In [34], an event-triggered bipartite time-varying formation control method was achieved for linear multi-agent systems with uncertain dynamics. Additionally, to further reduce the number of event triggers, researchers proposed a dynamic event-triggering strategy that introduces a dynamic variable for the static event-triggered strategy, allowing the triggering condition to change over time. In [35], a dynamic event-triggered strategy was proposed for the fixed-time consensus problem, reducing the number of event triggers in the system. In [36,37], bipartite consensus problems for multi-agent systems under dynamic event-triggered control were studied. However, ref. [35] did not account for competitive relationships among agents, and refs. [36,37] achieved only asymptotic consensus. Therefore, research on dynamic event-triggered fixed-time bipartite formation control for multi-agent systems remains highly important.

On the other hand, most control algorithms in [34–37] require continuous information measurement and transmission from the system. However, due to limited onboard communication and the actual hardware's driving capabilities, achieving real-time sampling and communication is difficult. To address these issues, researchers have combined periodic sampling [38–40] with event-triggered mechanisms, in which the core idea is to sample from continuous systems at specific times, with event detection occurring only on the sampled data. This approach accounts for the practical situation of periodic sensor sampling. It ensures that the minimum event-triggered interval is at least as long as the sampling interval, thereby further eliminating Zeno behavior. Currently, there is limited research on event-triggered consensus in sampled-data multi-agent systems. Reference [41] studied an event-triggered consensus problem for a class of nonlinear multi-agent systems based on sampled data. Reference [42] investigated a finite-time tracking consensus method for second-order multi-agent systems based on sampled data with an event-triggered scheme. Reference [43] formulated an asynchronous control problem of continuous-time positive Markov jump systems with a dynamic event-triggered scheme based on sampled data. However, the designs in [41,42] employ static event-triggered mechanisms, which can result in unnecessary triggering. Although ref. [43] proposed a dynamic event-triggered communication protocol, it did not account for competitive relationships among agents and did not achieve fixed-time consensus. Therefore, researching the dynamic event-triggered fixed-time convergence problem based on sampled data is a meaningful and challenging task.

Based on the above analysis, this paper addresses sampling periods, communication constraints, and fixed-time bipartite formation issues in multi-agent systems by proposing a dynamic event-triggered fixed-time bipartite consensus control algorithm using sampled data. The main contributions are summarized as follows:

(1) Design a periodic sampling mechanism. Compared to the existing algorithm in [36], it can reduce the system's communication frequency.

(2) Develop a dynamic event-triggered control algorithm based on sampled data to further reduce the communication burden compared with the existing algorithm in [42].

(3) Design a distributed fixed-time bipartite formation control method. Compared with the existing method in [43], the proposed method further accounts for competitive relationships among agents and converges faster.

Notations: $\mathbf{R}$, $\mathbf{R}^+$, $\mathbf{R}^N$, $\mathbf{R}^{N\times n}$, and $\mathbf{R}^{N\times N}$ represent the set of real numbers, positive real numbers, N-dimensional column vectors, $N \times n$-dimensional matrices, and N-dimensional square matrices, respectively.

2 Mathematical Preliminaries and Problem Statements

2.1 Signed Graph Theory

Consider an undirected graph $\mathcal{G} = (\mathcal{V}, \mathcal{E}, \mathcal{A})$ consisting of N nodes, where $\mathcal{V} = \{v_1, v_2, \ldots, v_N\}$ is the set of nodes of $\mathcal{G}$. Each node $v_i (i = 1, 2, \ldots, N)$ represents an agent i, and $\mathcal{E} \subseteq \mathcal{V} \times \mathcal{V}$ represents the set of edges. If $(v_i, v_j) \in \mathcal{E}$, it indicates that agent i can interact with neighbor agent j. $\mathcal{A} = [a_{ij}] \in \mathbf{R}^{N\times N}$ is the adjacency matrix of the graph $\mathcal{G}$. If $(v_i, v_j) \in \mathcal{E}$ and $i \neq j$ then $a_{ij} \neq 0$, otherwise, $a_{ij} = 0$. If there is a path between any pair of nodes in graph $\mathcal{G}$, then the graph is said to be connected. The node set $\mathcal{V}$ of the signed graph $\mathcal{G}$ can be partitioned into $\{\mathcal{V}_1, \mathcal{V}_2\}$, such that $\mathcal{V}_1 \cup \mathcal{V}_2 = \mathcal{V}$ and $\mathcal{V}_1 \cap \mathcal{V}_2 = \varnothing$. If all edges within $\mathcal{V}_1$ or $\mathcal{V}_2$ are positively weighted and all edges between $\mathcal{V}_1$ and $\mathcal{V}_2$ are negatively weighted, then the signed graph is structurally balanced. If $\forall v_i$ and $v_j \in \mathcal{V}_m (m \in \{1, 2\})$, then $a_{ij} \geq 0$. If $v_i \in \mathcal{V}_m$, $v_j \in \mathcal{V}_n$, and $m \neq n (m, n \in \{1, 2\})$, then $a_{ij} \leq 0$. The Laplacian matrix of the graph $\mathcal{G}$ is $\mathcal{L} = [l_{ij}] \in \mathbf{R}^{N\times N}$, where $l_{ii} = \sum_{i=1}^{N} |a_{ij}|$ and $l_{ij} = -a_{ij} (i \neq j)$. The $\mathcal{A}$ and $\mathcal{L}$ are both symmetric matrices.

2.2 Relevant Lemmas

Lemma 1 ([44]): *If there exists a continuous positive definite and radially unbounded function* $\Gamma : \boldsymbol{R}^n \to \boldsymbol{R}^+ \cup \{0\}$ *such that:*

(1) $\Gamma(x) = 0 \Leftrightarrow x = 0$;

(2) *For parameters* $\alpha, \beta > 0$, $p = 1 - \frac{1}{2r}$, $q = 1 + \frac{1}{2r}$, *and* $r > 1$, *if any solution* $x(t)$ *satisfies the inequality*

$$D^*\Gamma(x(t)) \leq -\alpha\Gamma^p(x(t)) - \beta\Gamma^q(x(t)) \tag{1}$$

the system's origin is globally fixed-time stable, and the settling time is obtained as

$$T \leq T_{\max} = \frac{\pi r}{\sqrt{\alpha\beta}}. \tag{2}$$

Lemma 2 ([27]): *If the signed graph* $\mathcal{G}$ *is structurally balanced, then there exists a diagonal matrix* $\boldsymbol{D} = diag\{d_1, d_2, \ldots, d_N\}$, *with* $d_i = \{\pm 1\}$, *such that* $\boldsymbol{D}\mathcal{A}\boldsymbol{D}$ *is nonnegative.*

Lemma 3 ([27]): *If the signed graph* $\mathcal{G}$ *is undirected and connected, then according to Lemma 2, it is obtained that the Laplacian matrix* $\mathcal{L}$ *of* $\mathcal{G}$ *is positive semi-definite, and its eigenvalues satisfy* $0 < \lambda_2 \leq \ldots \leq \lambda_N$. *The eigenvector corresponding to the eigenvalue* 0 *is* $\mathbf{1} = [1, 1, \ldots, 1]^T \in \boldsymbol{R}^N$. *Furthermore,* $\mathcal{G}$ *is a signed graph and*

structurally balanced. If $\mathbf{1}^T \boldsymbol{D}\boldsymbol{x} = 0$, *where* $\boldsymbol{x} = [x_1, x_2, \ldots, x_N]^T$, *then* $\lambda_2 \boldsymbol{x}^T\boldsymbol{x} \le \boldsymbol{x}^T\mathcal{L}\boldsymbol{x} \le \lambda_N \boldsymbol{x}^T\boldsymbol{x}$, *where* $\boldsymbol{x}^T\mathcal{L}\boldsymbol{x} = (1/2)\sum_{i=1}^{N}\sum_{j=1}^{N}\left|a_{ij}\right|(x_i - sign(a_{ij})x_j)^2$.

Lemma 4 ([35]): *For* $\ell_1, \ell_2, \ldots, \ell_m \ge 0$, $0 < p \le 1$, *and* $1 < q < \infty$, *we have*

$$m^{1-p}\left(\sum_{i=1}^{m}\ell_i\right)^p \ge \sum_{i=1}^{m}\ell_i{}^p \ge \left(\sum_{i=1}^{m}\ell_i\right)^p, m^{1-q}\left(\sum_{i=1}^{m}\ell_i\right)^q \le \sum_{i=1}^{m}\ell_i{}^q \le \left(\sum_{i=1}^{m}\ell_i\right)^q. \tag{3}$$

Remark 1: *Lemmas 1-4 are used to analyze the stability of the system controlled by our designed method, which is presented later. Moreover, it should be noted that Lemma 2 is a basic property for the signed graph* $\mathcal{G}$ *when it satisfies the structurally balanced condition, which ensures that the gauge transformation can be conducted and the Laplacian matrix* $\mathcal{L}$ *of the signed graph* $\mathcal{G}$ *is positive semi-definite. Further discussion can be found in [27,34], and [36].*

2.3 System Dynamics Descriptions

Consider a system composed of N agents, where i agent is described as

$$\begin{cases}\dot{x}_i(t) = u_i(t),\\ x(0) = x_0\end{cases} \tag{4}$$

where $x_i(t)$ represents the state of agent i, and $u_i(t)$ represents the control input of agent i.

Definition 1: *Let* $f = [f_1^T, f_2^T, \cdots, f_N^T]^T \in \boldsymbol{R}^{N\times n}$ *be the desired formation vector, where* $f_i = [f_{i1}, f_{i2}, \cdots, f_{in}]^T$. *The fixed-time bipartite formation of the multi-agent systems (4) implies there exists a prescribed time* T *such that* $\lim_{t\to T}\left\|x_i(t) - f_i - d_i d_j(x_j(t) - f_j)\right\| = 0$ *and for* $t \ge T$, *it satisfies* $\|x_i(t) - f_i\| = \left\|x_j(t) - f_j\right\|$. *The prescribed time* T *is bounded, and for any initial state of the system,* $\exists T_{\max} > 0$ *such that* $T \le T_{\max}$.

Assumption 1: *The communication topology* $\mathcal{G}$ *is undirected, connected, and structurally balanced.*

Remark 2: *A structurally balanced graph of the control systems' communication topology is a basic requirement of the controlled systems to realize bipartite formation control. As given in Section 2.1, this requirement is that all agents can be assigned to two distinct groups. The relationships within the same group are cooperative, but those between different groups are antagonistic. More deities are discussed in [27].*

2.4 Problem Statements

This study is focused on a class of continuous-time multi-agent systems to implement bipartite formation control tasks, where the main challenges are all listed as

(1) How to realize sampling control for the continuous system. Most existing methods are based on continuous systems and assume an infinite communication resource. In fact, when controlling the physical systems, we also need to detect the system and set a sampling time.

(2) How to realize dynamic event-triggered communication for the controlled system. Most existing methods are time-triggered or strictly event-triggered communication strategies, in which the event-triggered conditions are constant. Designing a dynamic event-triggered condition can further reduce the communication frequencies.

(3) How to realize fixed-time bipartite formation control for agents with a competitive relationship. Most existing formation control approaches consider only the cooperative relationships among agents. However, cooperative and competitive relationships coexist. Only considering one of the relationships is insufficient.

The objective of this study is to realize a sampling-based fixed-time dynamic event-triggered bipartite formation control method for a class of continuous-time multi-agent systems with cooperative and competitive relationships.

3 Main Results

For the multi-agent systems (4), the control law for the agent i is given as

$$u_i(t) = -a_1\Upsilon_i^{\mu}(t_k^i) - a_2\Upsilon_i^{\upsilon}(t_k^i) - a_3\Upsilon_i(t_k^i), t \in \left[t_k^i, t_{k+1}^i\right), \tag{5}$$

where a_1, a_2, and a_3 are all positive constants, $\mu > 1$, $0 < \upsilon < 1$, μ, and υ are ratios of two positive odd numbers, t_k^i represents the triggering time of agent i, and t_{k+1}^i represents the next triggering time of agent i. Moreover, $k = 1, 2, \ldots$ represents the specific number of triggers. $\Upsilon_i(t)$ is defined as $\Upsilon_i(t) = \sum_{j=1}^{N} \left|a_{ij}\right| (\hat{x}_i(t) - sign(a_{ij})\hat{x}_j(t))$, where $\hat{x}_i(t) = x_i(t) - f_i, i = 1, 2, \ldots, N$. Then, we have $\boldsymbol{\Upsilon}(t) = \left[\Upsilon_1(t), \Upsilon_2(t), \ldots, \Upsilon_N(t)\right]^{\mathrm{T}} = \mathcal{L}\hat{\boldsymbol{x}}$, where $\hat{\boldsymbol{x}} = \left[\hat{x}_1, \hat{x}_2, \ldots, \hat{x}_N\right]^{\mathrm{T}}$.

To reduce the real-time computation burden of the system, a combined measurement error equation based on periodic sampling is designed as

$$\begin{aligned}\Delta_i(t_k^i + mh) = {} & a_1\Upsilon_i^{\mu}(t_k^i) + a_2\Upsilon_i^{\upsilon}(t_k^i) + a_3\Upsilon_i(t_k^i) - a_1\Upsilon_i^{\mu}(t_k^i + mh) - a_2\Upsilon_i^{\upsilon}(t_k^i + mh) \\ & - a_3\Upsilon_i(t_k^i + mh),\end{aligned} \tag{6}$$

where $m = 1, 2, \ldots$, and $h > 0$ is the synchronous sampling period of the agents. Combining Eqs. (6) with (5), we get that

$$u_i(t) = -\Delta_i(t_k^i + mh) - a_1\Upsilon_i^{\mu}(t_k^i + mh) - a_2\Upsilon_i^{\upsilon}(t_k^i + mh) - a_3\Upsilon_i(t_k^i + mh). \tag{7}$$

The compact form of Eq. (7) for $t \in [kh, kh + h)$ is $u_i(t) = -\Delta_i(kh) - a_1\Upsilon_i^{\mu}(kh) - a_2\Upsilon_i^{\upsilon}(kh) - a_3\Upsilon_i(kh)$. Hence, it follows that

$$\dot{\hat{x}}(t) = -\boldsymbol{\Delta}(kh) - a_1\boldsymbol{\Upsilon}^{\mu}(kh) - a_2\boldsymbol{\Upsilon}^{\upsilon}(kh) - a_3\boldsymbol{\Upsilon}(kh), \tag{8}$$

where $\boldsymbol{\Delta} = \left[\Delta_1, \Delta_2, \ldots, \Delta_N\right]^{\mathrm{T}}$.

To further reduce the number of event triggers, the dynamic event-triggered condition for agent i is designed as

$$\tau(\Delta_i^2(kh) - b_1\Upsilon_i^{2\mu}(kh) - b_2\Upsilon_i^{2\upsilon}(kh)) \geq \Phi_i^{\frac{\mu+1}{2}}(kh) + \Phi_i^{\frac{\upsilon+1}{2}}(kh), \tag{9}$$

where τ, b_1, and b_2 are positive design parameters. Moreover, Φ_i is the internal dynamic variable, and we have

$$\dot{\Phi}_i(t) = -c_1\Phi_i^{\frac{\mu+1}{2}}(kh) - c_2\Phi_i^{\frac{\upsilon+1}{2}}(kh) + \sigma(b_1\Upsilon_i^{2\mu}(kh) + b_2\Upsilon_i^{2\upsilon}(kh) - \Delta_i^2(kh)), \tag{10}$$

where $\Phi_i(0) > 0$ and $t \in [kh, kh + h)$. Moreover, c_1 and c_2 are positive constants, and $\sigma \in (0, 1)$ is a design parameter.

From Eqs. (9) and (10), we get that

$$\dot{\Phi}_i(t) \geq -\left(c_1 + \frac{\sigma}{\tau}\right)\Phi_i^{\frac{\mu+1}{2}}(kh) - \left(c_2 + \frac{\sigma}{\tau}\right)\Phi_i^{\frac{\upsilon+1}{2}}(kh). \tag{11}$$

According to reference [35], we consider a function as

$$\dot{\Phi}_i(t) \geq -\left(c_1 + \frac{\sigma}{\tau}\right)\Phi_i^{\frac{\mu+1}{2}}(t) - \left(c_2 + \frac{\sigma}{\tau}\right)\Phi_i^{\frac{v+1}{2}}(t). \tag{12}$$

when $t \geq 0$, we have $\Phi_i(t) \geq e^{\int_0^t \varphi(s)ds}\Phi_i(0) > 0$, with $\varphi(t) = -(c_1 + \frac{\sigma}{\tau})\Phi_i^{\frac{\mu-1}{2}}(t) - (c_2 + \frac{\sigma}{\tau})\Phi_i^{\frac{v-1}{2}}(t)$. Hence, the sample of $\Phi_i(t)$ results in $\Phi_i(kh) > 0$.

When the dynamic event-triggered condition (9) is satisfied, the controller updates its value using the neighbor agent's state at the triggering time. When the triggering condition is not satisfied, the system employs a zero-order holder (ZOH) to maintain the controller's output at the control value from the previous trigger time.

In summary, a sampling-based dynamic event-triggered fixed-time bipartite formation algorithm is schematically outlined in Fig. 1.

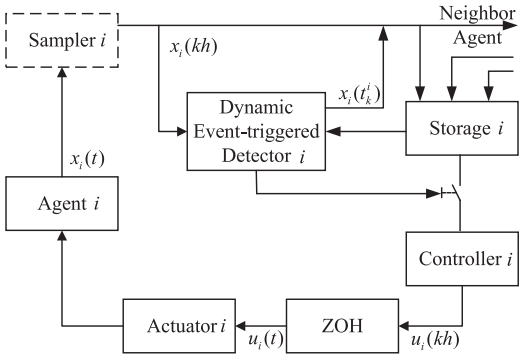

Figure 1: Diagram of the designed control method.

Remark 3: *From Eqs. (9) and (10), it is found that the left items* $\tau(\Delta_i^2(kh) - b_1\Upsilon_i^{2\mu}(kh) - b_2\Upsilon_i^{2v}(kh))$ *is similar to the right items* $\sigma(b_1\Upsilon_i^{2\mu}(kh) + b_2\Upsilon_i^{2v}(kh) - \Delta_i^2(kh))$ *in Eq. (9). However, Eq. (10) includes extra negative items* $-c_1\Phi_i^{\frac{\mu+1}{2}}(kh) - c_2\Phi_i^{\frac{v+1}{2}}(kh)$*, which can further ensure that the condition (9) holds at early states. When the controlled systems achieve stability, the left-hand side of Eq. (9) converges to the origin, but the condition (9) is not satisfied. In other words, at the early stage, communication is more frequent to facilitate rapid convergence, whereas during the transition to stability, it is reduced to prevent unnecessary triggering.*

Remark 4: *Reference [36] uses continuous state information* $x_i(t)$ *of agent i under ideal conditions, assuming that agents can obtain and transmit information at any moment, without considering that actual embedded systems can only sample and communicate based on a fixed period dictated by the clock. This paper examines the impact of the sensor sampling period on the system, using sampled data* $x_i(kh)$ *that more closely reflect real-world conditions and align with the operational mechanisms of actual systems. Each agent's state is sampled at a fixed sampling period h and transmitted to neighboring agents and the dynamic event-triggered detector, where the range of the sampling period is provided in the following sections. Since the event detection is based on sampled data,* $x_i(t_k^i)$ *is a subset of* $x_i(kh)$ *and* $\{t_0^i, t_1^i, t_2^i, \ldots\} \subseteq \{0, h, 2h, \ldots\}$*. The minimum value of* $t_{k+1}^i - t_k^i$ *is one sampling period h, which excludes Zeno behavior.*

Theorem 1: *When the following conditions are satisfied:*

$$h(a_3^2 + a_3 + a_1a_3 + a_2a_3)\lambda_N < a_3 - \frac{1}{4}, \tag{13}$$

$$h(a_1 + a_2 + a_3 + 1)\lambda_N < g_0\tau + \sigma - 1, \tag{14}$$

$$\sqrt{g_1(2\lambda_N)^{\mu}} < a_1 N^{\frac{1-\mu}{2}}(2\lambda_2)^{\frac{\mu+1}{2}}, \tag{15}$$

$$\sqrt{g_2 N^{1-\upsilon}(2\lambda_N)^{\upsilon}} < a_2(2\lambda_2)^{\frac{\upsilon+1}{2}}, \tag{16}$$

where $g_0 = \min\{c_1, c_2\}$, $g_1 = h(b_1 + a_1b_1 + a_2b_1 + a_3b_1 + a_1 + a_1^2 + a_1a_2 + a_1a_3)\lambda_N + b_1$, *and* $g_2 = h(b_2 + a_1b_2 + a_2b_2 + a_3b_2 + a_2 + a_2^2 + a_1a_2 + a_2a_3)\lambda_N + b_2$, *using the above control and triggering conditions, the multi-agent system (4) can achieve fixed-time bipartite formation within a specific sampling period range.*

Proof: Consider a Lyapunov function as

$$V(t) = \frac{1}{2}\hat{\boldsymbol{x}}^{\mathrm{T}}(t)\mathcal{L}\hat{\boldsymbol{x}}(t) + \sum_{i=1}^{N}\Phi_i(t), t \in [kh, kh+h). \tag{17}$$

Let $V_1(t) = \frac{1}{2}\hat{\boldsymbol{x}}^{\mathrm{T}}(t)\mathcal{L}\hat{\boldsymbol{x}}(t)$ and $V_2(t) = \sum_{i=1}^{N}\Phi_i(t)$, then $V(t) = V_1(t) + V_2(t)$. From the above, we know $V_1(t) \geq 0$ and $V_2(t) > 0$, so $V(t) \geq 0$. For convenience, let $kh = \kappa$. The derivative of $V(t)$ is

$$\begin{aligned}
\dot{V}(t) &= \hat{\boldsymbol{x}}^{\mathrm{T}}(t)\mathcal{L}\dot{\hat{x}}(t) + \sum_{i=1}^{N}\dot{\Phi}_i(t) \\
&= (\hat{\boldsymbol{x}}(\kappa) + (t-\kappa)(-\boldsymbol{\Delta}(\kappa) - a_1\boldsymbol{\Upsilon}^{\mu}(\kappa) - a_2\boldsymbol{\Upsilon}^{\upsilon}(\kappa) - a_3\boldsymbol{\Upsilon}(\kappa)))^{\mathrm{T}}\mathcal{L} \\
&\quad \times (-\boldsymbol{\Delta}(\kappa) - a_1\boldsymbol{\Upsilon}^{\mu}(\kappa) - a_2\boldsymbol{\Upsilon}^{\upsilon}(\kappa) - a_1\boldsymbol{\Upsilon}(\kappa)) - c_1\sum_{i=1}^{N}\Phi_i^{\frac{\mu+1}{2}}(\kappa) - c_2\sum_{i=1}^{N}\Phi_i^{\frac{\upsilon+1}{2}}(\kappa) \\
&\quad + \sigma(b_1\boldsymbol{\Upsilon}^{\mu}(\kappa)^{\mathrm{T}}\boldsymbol{\Upsilon}^{\mu}(\kappa) + b_2\boldsymbol{\Upsilon}^{\upsilon}(\kappa)^{\mathrm{T}}\boldsymbol{\Upsilon}^{\upsilon}(\kappa) - \boldsymbol{\Delta}^{\mathrm{T}}(\kappa)\boldsymbol{\Delta}(\kappa)) \\
&\quad \leq -\boldsymbol{\Upsilon}^{\mathrm{T}}(\kappa)\boldsymbol{\Delta}(\kappa) - a_1\boldsymbol{\Upsilon}^{\mathrm{T}}(\kappa)\boldsymbol{\Upsilon}^{\mu}(\kappa) - a_2\boldsymbol{\Upsilon}^{\mathrm{T}}(\kappa)\boldsymbol{\Upsilon}^{\upsilon}(\kappa) - a_3\boldsymbol{\Upsilon}^{\mathrm{T}}(\kappa)\boldsymbol{\Upsilon}(\kappa) \\
&\quad + h(\boldsymbol{\Delta}^{\mathrm{T}}(\kappa)\mathcal{L}\boldsymbol{\Delta}(\kappa) + a_1^2\boldsymbol{\Upsilon}^{\mu}(\kappa)^{\mathrm{T}}\mathcal{L}\boldsymbol{\Upsilon}^{\mu}(\kappa) + a_2^2\boldsymbol{\Upsilon}^{\upsilon}(\kappa)^{\mathrm{T}}\mathcal{L}\boldsymbol{\Upsilon}^{\upsilon}(\kappa) \\
&\quad + a_3^2\boldsymbol{\Upsilon}^{\mathrm{T}}(\kappa)\mathcal{L}\boldsymbol{\Upsilon}(\kappa) + 2a_1\boldsymbol{\Delta}^{\mathrm{T}}(\kappa)\mathcal{L}\boldsymbol{\Upsilon}^{\mu}(\kappa) + 2a_2\boldsymbol{\Delta}^{\mathrm{T}}(\kappa)\mathcal{L}\boldsymbol{\Upsilon}^{\upsilon}(\kappa) + 2a_3\boldsymbol{\Delta}^{\mathrm{T}}(\kappa)\mathcal{L}\boldsymbol{\Upsilon}(\kappa) \\
&\quad + 2a_1a_2\boldsymbol{\Upsilon}^{\mu}(\kappa)^{\mathrm{T}}\mathcal{L}\boldsymbol{\Upsilon}^{\upsilon}(\kappa) + 2a_1a_3\boldsymbol{\Upsilon}^{\mu}(\kappa)^{\mathrm{T}}\mathcal{L}\boldsymbol{\Upsilon}(\kappa) + 2a_2a_3\boldsymbol{\Upsilon}^{\upsilon}(\kappa)^{\mathrm{T}}\mathcal{L}\boldsymbol{\Upsilon}(\kappa)) \\
&\quad - c_1\sum_{i=1}^{N}\Phi_i^{\frac{\mu+1}{2}}(\kappa) - c_2\sum_{i=1}^{N}\Phi_i^{\frac{\upsilon+1}{2}}(\kappa) + \sigma(b_1\boldsymbol{\Upsilon}^{\mu}(\kappa)^{\mathrm{T}}\boldsymbol{\Upsilon}^{\mu}(\kappa) + b_2\boldsymbol{\Upsilon}^{\upsilon}(\kappa)^{\mathrm{T}}\boldsymbol{\Upsilon}^{\upsilon}(\kappa) - \boldsymbol{\Delta}^{\mathrm{T}}(\kappa)\boldsymbol{\Delta}(\kappa)).
\end{aligned} \tag{18}$$

Combine Lemma 3 and the following inequality

$$\boldsymbol{a}^{\mathrm{T}}\mathcal{L}\boldsymbol{b} \leq \frac{1}{2}\boldsymbol{a}^{\mathrm{T}}\mathcal{L}\boldsymbol{a} + \frac{1}{2}\boldsymbol{b}^{\mathrm{T}}\mathcal{L}\boldsymbol{b}, \forall \boldsymbol{a}, \boldsymbol{b} \in \boldsymbol{R}^n. \tag{19}$$

Then, we obtain that

$$\begin{aligned}
\dot{V}(t) &\leq \left|\boldsymbol{\Upsilon}^{\mathrm{T}}(\kappa)\right||\boldsymbol{\Delta}(\kappa)| - a_1\boldsymbol{\Upsilon}^{\mathrm{T}}(\kappa)\boldsymbol{\Upsilon}^{\mu}(\kappa) - a_2\boldsymbol{\Upsilon}^{\mathrm{T}}(\kappa)\boldsymbol{\Upsilon}^{\upsilon}(\kappa) - a_3\boldsymbol{\Upsilon}^{\mathrm{T}}(\kappa)\boldsymbol{\Upsilon}(\kappa) \\
&\quad + h(1 + a_1 + a_2 + a_3)\lambda_N\boldsymbol{\Delta}^{\mathrm{T}}(\kappa)\boldsymbol{\Delta}(\kappa) + h(a_1 + a_1^2 + a_1a_2 + a_1a_3)\lambda_N\boldsymbol{\Upsilon}^{\mu}(\kappa)^{\mathrm{T}}\boldsymbol{\Upsilon}^{\mu}(\kappa) \\
&\quad + h(a_2 + a_2^2 + a_1a_2 + a_2a_3)\lambda_N\boldsymbol{\Upsilon}^{\upsilon}(\kappa)^{\mathrm{T}}\boldsymbol{\Upsilon}^{\upsilon}(\kappa) + h(a_3 + a_3^2 + a_1a_3 + a_2a_3)\lambda_N\boldsymbol{\Upsilon}^{\mathrm{T}}(\kappa)\boldsymbol{\Upsilon}(\kappa) \\
&\quad - c_1\sum_{i=1}^{N}\Phi_i^{\frac{\mu+1}{2}}(\kappa) - c_2\sum_{i=1}^{N}\Phi_i^{\frac{\upsilon+1}{2}}(\kappa) + \sigma(b_1\boldsymbol{\Upsilon}^{\mu}(\kappa)^{\mathrm{T}}\boldsymbol{\Upsilon}^{\mu}(\kappa) + b_2\boldsymbol{\Upsilon}^{\upsilon}(\kappa)^{\mathrm{T}}\boldsymbol{\Upsilon}^{\upsilon}(\kappa) - \boldsymbol{\Delta}^{\mathrm{T}}(\kappa)\boldsymbol{\Delta}(\kappa)) \\
&\quad \leq \left(\frac{1}{4} - a_3 + h(a_3 + a_3^2 + a_1a_3 + a_2a_3)\lambda_N\right)\boldsymbol{\Upsilon}^{\mathrm{T}}(\kappa)\boldsymbol{\Upsilon}(\kappa) - a_1\boldsymbol{\Upsilon}^{\mathrm{T}}(\kappa)\boldsymbol{\Upsilon}^{\mu}(\kappa) - a_2\boldsymbol{\Upsilon}^{\mathrm{T}}(\kappa)\boldsymbol{\Upsilon}^{\upsilon}(\kappa) \\
&\quad + \boldsymbol{\Delta}^{\mathrm{T}}(\kappa)\boldsymbol{\Delta}(\kappa) + h(1 + a_1 + a_2 + a_3)\lambda_N\boldsymbol{\Delta}^{\mathrm{T}}(\kappa)\boldsymbol{\Delta}(\kappa) + h(a_1 + a_1^2 + a_1a_2 + a_1a_3)\lambda_N\boldsymbol{\Upsilon}^{\mu}(\kappa)^{\mathrm{T}}\boldsymbol{\Upsilon}^{\mu}(\kappa)
\end{aligned}$$

$$+ h(a_2 + a_2^2 + a_1a_2 + a_2a_3)\lambda_N \boldsymbol{\Upsilon}^{\upsilon}(\kappa)^{\mathrm{T}}\boldsymbol{\Upsilon}^{\upsilon}(\kappa) - c_1\sum_{i=1}^{N}\Phi_i^{\frac{\mu+1}{2}}(\kappa) - c_2\sum_{i=1}^{N}\Phi_i^{\frac{\upsilon+1}{2}}(\kappa)$$
$$+ \sigma(b_1\boldsymbol{\Upsilon}^{\mu}(\kappa)^{\mathrm{T}}\boldsymbol{\Upsilon}^{\mu}(\kappa) + b_2\boldsymbol{\Upsilon}^{\upsilon}(\kappa)^{\mathrm{T}}\boldsymbol{\Upsilon}^{\upsilon}(\kappa) - \boldsymbol{\Delta}^{\mathrm{T}}(\kappa)\boldsymbol{\Delta}(\kappa)). \tag{20}$$

when conditions (13)–(16) are met, we get that

$$\begin{aligned}\dot{V}(t) &\le -a_1\boldsymbol{\Upsilon}^{\mathrm{T}}(\kappa)\boldsymbol{\Upsilon}^{\mu}(\kappa) - a_2\boldsymbol{\Upsilon}^{\mathrm{T}}(\kappa)\boldsymbol{\Upsilon}^{\upsilon}(\kappa) + \boldsymbol{\Delta}^{\mathrm{T}}(\kappa)\boldsymbol{\Delta}(\kappa) + h(1+a_1+a_2+a_3)\lambda_N\boldsymbol{\Delta}^{\mathrm{T}}(\kappa)\boldsymbol{\Delta}(\kappa)\\
&\quad + h(a_1 + a_1^2 + a_1a_2 + a_1a_3)\lambda_N\boldsymbol{\Upsilon}^{\mu}(\kappa)^{\mathrm{T}}\boldsymbol{\Upsilon}^{\mu}(\kappa) + h(a_2 + a_2^2 + a_1a_2 + a_2a_3)\lambda_N\boldsymbol{\Upsilon}^{\upsilon}(\kappa)^{\mathrm{T}}\boldsymbol{\Upsilon}^{\upsilon}(\kappa)\\
&\quad - c_1\sum_{i=1}^{N}\Phi_i^{\frac{\mu+1}{2}}(\kappa) - c_2\sum_{i=1}^{N}\Phi_i^{\frac{\upsilon+1}{2}}(\kappa) + \sigma(b_1\boldsymbol{\Upsilon}^{\mu}(\kappa)^{\mathrm{T}}\boldsymbol{\Upsilon}^{\mu}(\kappa) + b_2\boldsymbol{\Upsilon}^{\upsilon}(\kappa)^{\mathrm{T}}\boldsymbol{\Upsilon}^{\upsilon}(\kappa) - \boldsymbol{\Delta}^{\mathrm{T}}(\kappa)\boldsymbol{\Delta}(\kappa))\\
&\le -a_1\boldsymbol{\Upsilon}^{\mathrm{T}}(\kappa)\boldsymbol{\Upsilon}^{\mu}(\kappa) - a_2\boldsymbol{\Upsilon}^{\mathrm{T}}(\kappa)\boldsymbol{\Upsilon}^{\upsilon}(\kappa) + h(1+a_1+a_2+a_3)\lambda_N\boldsymbol{\Delta}^{\mathrm{T}}(\kappa)\boldsymbol{\Delta}(\kappa)\\
&\quad + (h(a_1 + a_1^2 + a_1a_2 + a_1a_3)\lambda_N + b_1)\boldsymbol{\Upsilon}^{\mu}(\kappa)^{\mathrm{T}}\boldsymbol{\Upsilon}^{\mu}(\kappa)\\
&\quad + (h(a_2 + a_2^2 + a_1a_2 + a_2a_3)\lambda_N + b_2)\boldsymbol{\Upsilon}^{\upsilon}(\kappa)^{\mathrm{T}}\boldsymbol{\Upsilon}^{\upsilon}(\kappa) - c_1\sum_{i=1}^{N}\Phi_i^{\frac{\mu+1}{2}}(\kappa) - c_2\sum_{i=1}^{N}\Phi_i^{\frac{\upsilon+1}{2}}(\kappa)\\
&\quad + (\sigma-1)(b_1\boldsymbol{\Upsilon}^{\mu}(\kappa)^{\mathrm{T}}\boldsymbol{\Upsilon}^{\mu}(\kappa) + b_2\boldsymbol{\Upsilon}^{\upsilon}(\kappa)^{\mathrm{T}}\boldsymbol{\Upsilon}^{\upsilon}(\kappa) - \boldsymbol{\Delta}^{\mathrm{T}}(\kappa)\boldsymbol{\Delta}(\kappa)).\end{aligned} \tag{21}$$

Combining the dynamic event-triggered condition (9), we obtain that

$$\begin{aligned}\dot{V}(t) &\le -a_1\boldsymbol{\Upsilon}^{\mathrm{T}}(\kappa)\boldsymbol{\Upsilon}^{\mu}(\kappa) - a_2\boldsymbol{\Upsilon}^{\mathrm{T}}(\kappa)\boldsymbol{\Upsilon}^{\upsilon}(\kappa) + g_1\boldsymbol{\Upsilon}^{\mu}(\kappa)^{\mathrm{T}}\boldsymbol{\Upsilon}^{\mu}(\kappa) + g_2\boldsymbol{\Upsilon}^{\upsilon}(\kappa)^{\mathrm{T}}\boldsymbol{\Upsilon}^{\upsilon}(\kappa)\\
&\quad - \left(c_1 - \frac{1-\sigma+h(1+a_1+a_2+a_3)\lambda_N}{\tau}\right)\sum_{i=1}^{N}\Phi_i^{\frac{\mu+1}{2}}(\kappa)\\
&\quad - \left(c_2 - \frac{1-\sigma+h(1+a_1+a_2+a_3)\lambda_N}{\tau}\right)\sum_{i=1}^{N}\Phi_i^{\frac{\upsilon+1}{2}}(\kappa).\end{aligned} \tag{22}$$

From Lemma 4, we derive that

$$\boldsymbol{\Upsilon}^{\mathrm{T}}(\kappa)\boldsymbol{\Upsilon}^{\mu}(\kappa) = \sum_{i=1}^{N}\Upsilon_i^{\mu+1}(\kappa) = \sum_{i=1}^{N}(\Upsilon_i^2(\kappa))^{\frac{\mu+1}{2}} \ge N^{\frac{1-\mu}{2}}\left(\sum_{i=1}^{N}\Upsilon_i^2(\kappa)\right). \tag{23}$$

and

$$\begin{aligned}\sum_{i=1}^{N}\Upsilon_i^2(\kappa) &= \boldsymbol{\Upsilon}^{\mathrm{T}}(\kappa)\boldsymbol{\Upsilon}(\kappa) = (\mathcal{L}\hat{\boldsymbol{x}})^{\mathrm{T}}(\mathcal{L}\hat{\boldsymbol{x}}) = \hat{\boldsymbol{x}}^{\mathrm{T}}\mathcal{L}^2\hat{\boldsymbol{x}}\\
&= (\mathcal{L}^{\frac{1}{2}}\hat{\boldsymbol{x}})^{\mathrm{T}}\mathcal{L}(\mathcal{L}^{\frac{1}{2}}\hat{\boldsymbol{x}}) \ge \lambda_2\hat{\boldsymbol{x}}^{\mathrm{T}}\mathcal{L}\hat{\boldsymbol{x}} = 2\lambda_2 V_1.\end{aligned} \tag{24}$$

By substituting Eq. (24) into Eq. (23), we get that

$$\boldsymbol{\Upsilon}^{\mathrm{T}}(\kappa)\boldsymbol{\Upsilon}^{\mu}(\kappa) \ge N^{\frac{1-\mu}{2}}(2\lambda_2 V_1)^{\frac{\mu+1}{2}}. \tag{25}$$

Similarly, we obtain that

$$\begin{aligned}&\boldsymbol{\Upsilon}^{\mathrm{T}}(\kappa)\boldsymbol{\Upsilon}^{\upsilon}(\kappa) \ge (2\lambda_2 V_1)^{\frac{\upsilon+1}{2}}\\
&\boldsymbol{\Upsilon}^{\mu}(\kappa)^{\mathrm{T}}\boldsymbol{\Upsilon}^{\mu}(\kappa) \le (2\lambda_N V_1)^{\mu}\\
&\boldsymbol{\Upsilon}^{\upsilon}(\kappa)^{\mathrm{T}}\boldsymbol{\Upsilon}^{\upsilon}(\kappa) \le N^{1-\upsilon}(2\lambda_N V_1).\end{aligned} \tag{26}$$

Substituting Eqs. (25) and (26) into Eq. (22), and combining them with Lemma 4, we get that

$$\begin{aligned}\dot{V}(t) \le & -a_1 N^{\frac{1-\mu}{2}}(2\lambda_2)^{\frac{\mu+1}{2}} V_1^{\frac{\mu+1}{2}} - a_2(2\lambda_2)^{\frac{\upsilon+1}{2}} V_1^{\frac{\upsilon+1}{2}} + \left(\sqrt{g_1(2\lambda_N)^{\mu}} V_1^{\frac{\mu}{2}}\right)^2 + \left(\sqrt{g_2 N^{1-\upsilon}(2\lambda_N)^{\upsilon}} V_1^{\frac{\upsilon}{2}}\right)^2 \\ & - N^{\frac{1-\mu}{2}}\left(c_1 - \frac{1-\sigma+h(1+a_1+a_2+a_3)\lambda_N}{\tau}\right) V_2^{\frac{\mu+1}{2}} \\ & - \left(c_2 - \frac{1-\sigma+h(1+a_1+a_2+a_3)\lambda_N}{\tau}\right) V_2^{\frac{\upsilon+1}{2}}. \end{aligned} \tag{27}$$

when conditions (15) and (16) are satisfied, we get that

$$\begin{aligned}\dot{V}(t) &\le -g_3\left(V_1^{\frac{\mu+1}{2}} + V_2^{\frac{\mu+1}{2}}\right) - g_4\left(V_1^{\frac{\upsilon+1}{2}} + V_2^{\frac{\upsilon+1}{2}}\right) \\ &\le -g_3 2^{\frac{1-\mu}{2}} V^{\frac{\mu+1}{2}} - g_4 V^{\frac{\upsilon+1}{2}}. \end{aligned} \tag{28}$$

where $g_3 = \min\{a_1 N^{\frac{1-\mu}{2}}(2\lambda_2)^{\frac{\mu+1}{2}}, N^{\frac{1-\mu}{2}}(c_1 - \frac{1-\sigma+h(1+a_1+a_2+a_3)\lambda_N}{\tau})\}$, and $g_4 = \min\{a_2(2\lambda_2)^{\frac{\upsilon+1}{2}}, c_2 - \frac{1-\delta+h(1+a_1+a_2+a_3)\lambda_N}{\tau}\}$.

From Eq. (28) and Lemma 1, we conclude that the multi-agent systems (4) can achieve fixed-time bipartite formation, with the settling time as

$$T \le T_{\max} = \frac{\pi}{(\mu-1)\sqrt{2^{\frac{1-\mu}{2}} g_3 g_4}} \tag{29}$$

Since the agent's event detection occurs within the sampling period h, the minimum interval for triggering an event is h, thereby fundamentally eliminating the Zeno phenomenon.□

4 Simulation Analysis

4.1 Example 1

Consider a system composed of seven agents, with the communication topology shown in Fig. 2, where solid lines represent cooperative relationships and dashed lines indicate competitive relationships. From Fig. 2, it is obtained that the second smallest eigenvalue of $\mathcal{L}$ is $\lambda_2 = 0.75$, and the largest eigenvalue is $\lambda_N = 3.80$. The initial state and initial dynamic variable values of the system are $x(0) = \begin{bmatrix} -16 & -25 & -10 & 0 & 6 & 20 & 11 \end{bmatrix}^{\mathrm{T}}$ and $\Phi_i(0) = 40$. The parameters in Eqs. (5), (9) and (10) are designed as $a_1 = 3$, $a_2 = 1$, $a_3 = 1$, $\mu = 11/9$, $\upsilon = 7/9$, $f_1 = -1$, $f_2 = -2$, $f_3 = 1$, $f_4 = 2$, $f_5 = 3$, $f_6 = 4$, $f_7 = -3$, $b_1 = 0.09$, $b_2 = 0.01$, $c_1 = 1$, $c_2 = 1$, $\sigma = 0.01$, and $\tau = 10$. Using these design parameters and Eq. (2), the settling time is $T \le T_{\max} = 18.6$ s, where $T_{\max}$ is the maximum settling time, providing an upper bound estimate. From Theorem 1, the system's sampling period can be ensured to be within $h \le 0.033$ s.

When $h = 0.01$ s, under the same parameters, the state evolution and triggering instants of the system using different sampled-data-based event-triggered mechanisms are illustrated in Fig. 3. According to reference [42], the static event triggering condition is designed as $\Delta_i^2(kh) - b_1\Upsilon_i^{2\mu}(kh) - b_2\Upsilon_i^{2\upsilon}(kh) \ge 0$. From Fig. 3, it can be observed that under nearly identical convergence rates, the number of triggers for agents 1–7 under dynamic event-triggered strategy are 20, 23, 23, 22, 18, 12, and 20, respectively, whereas under static event-triggered strategy, the triggers are 76, 77, 81, 79, 72, 72, and 71, respectively. Compared to the static event-triggered strategy in [42], the dynamic event-triggered strategy proposed in this paper can further reduce the number of triggers by 73.8%, thereby reducing the system's communication resources.

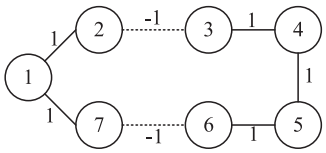

Figure 2: Communication topology of the controlled multi-agent systems.

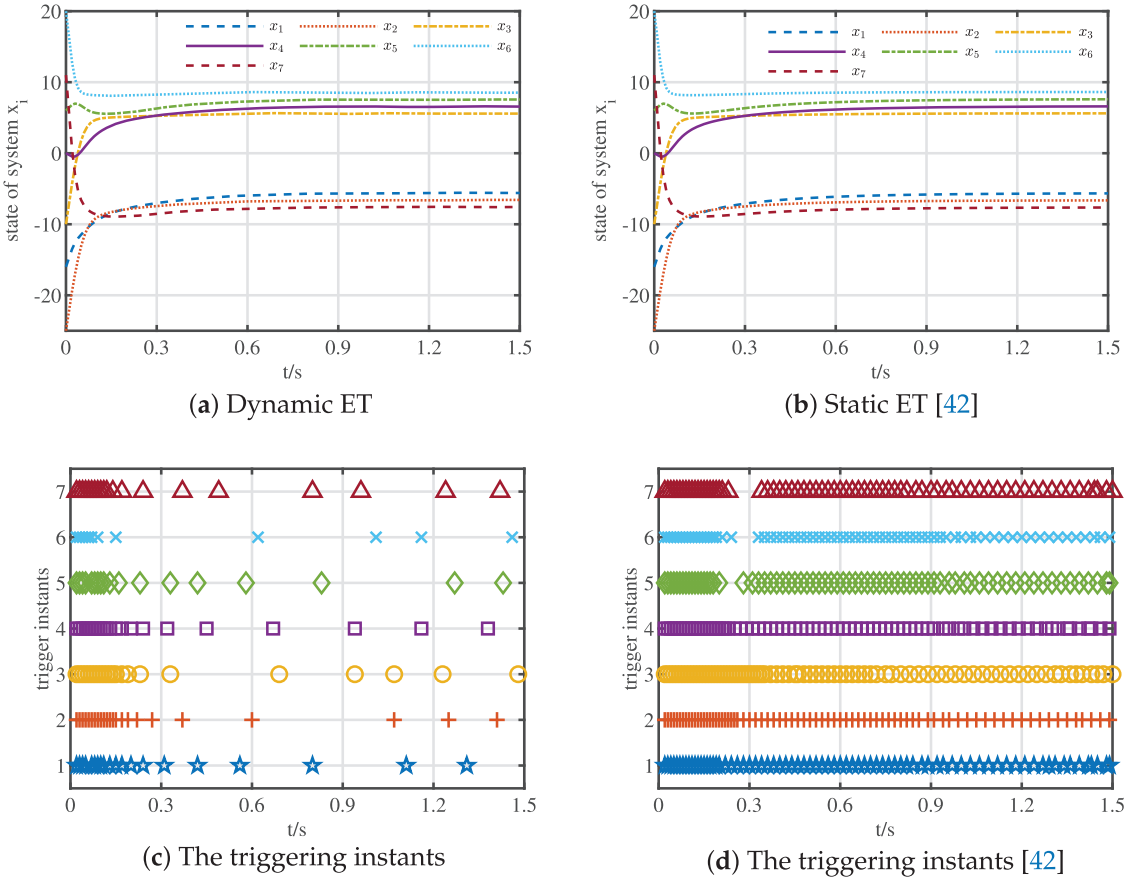

(**a**) Dynamic ET (**b**) Static ET [42]

(**c**) The triggering instants (**d**) The triggering instants [42]

Figure 3: Fixed-time bipartite formation using different event-triggered mechanisms.

Furthermore, this paper conducts simulations with varying sampling periods, as shown in Fig. 4. The effectiveness is characterized by $V_1(t) = 0.5\boldsymbol{x}^{\mathrm{T}}(t)\mathcal{L}\boldsymbol{x}(t)$. Fig. 4 shows that: (1) With a smaller sampling period, event detection frequency is higher, and the controller updates more frequently, allowing timely adjustment of the system state. Thus, the collection process is smoother with less fluctuation. However, shorter sampling periods increase computational requirements, making real-time implementation more difficult. (2) With a larger sampling period, event detection frequency is lower, and the trigger count decreases. However, as the sampling period approaches a stable value, the controller cannot adjust the system state in time, leading to poor system effectiveness because the event triggering condition is often not satisfied, thereby increasing the trigger count. Therefore, selecting an appropriate sampling period is critical to the stability of real systems and to the number of triggers, which is one of the research objectives of this paper.

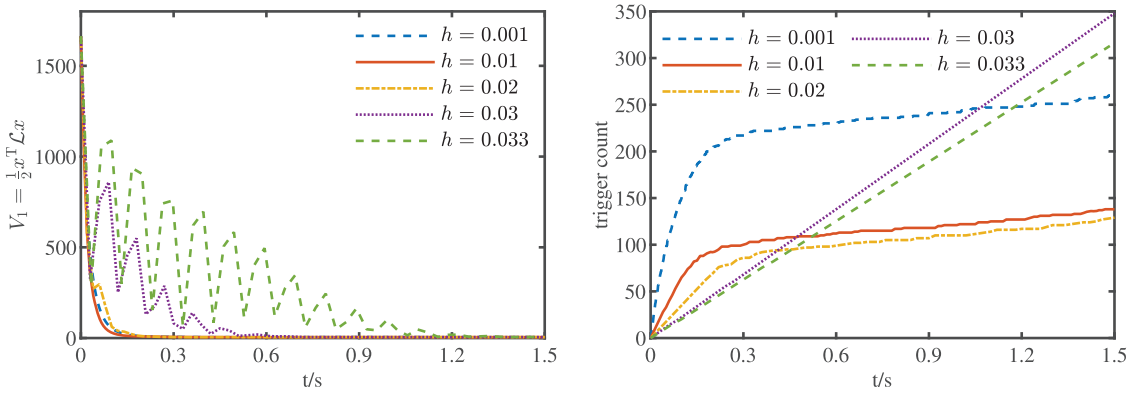

(**a**) The convergence effect (**b**) The trigger count

Figure 4: The impact of different sampling periods on the controlled multi-agent systems.

Finally, to verify the superiority of this algorithm, a comparative experiment with the existing method in [43] was conducted, and the results are shown in Fig. 5. Figs. 3a and 5a are the same. Fig. 5c changes the initial state to $x'(0) = \begin{bmatrix} -180 & -290 & -110 & 0 & 80 & 230 & 120 \end{bmatrix}^{\mathrm{T}}$ and the initial dynamic variable value to $\Phi_i(0) = 500$ and $\sigma = 0.001$, with other parameters as in Fig. 5a. Comparing Fig. 5b and d, the collection time of the algorithm in reference [43] increases with the increase in the initial state. In contrast, the upper bound on the algorithm's collection time in this paper is independent of the initial state. Comparing Fig. 5a and b, with the same initial state, the actual states coincide at $t = 0.9$ s and $t = 7$ s, indicating that the algorithm in this paper has a faster convergence speed compared to the existing algorithm in reference [43].

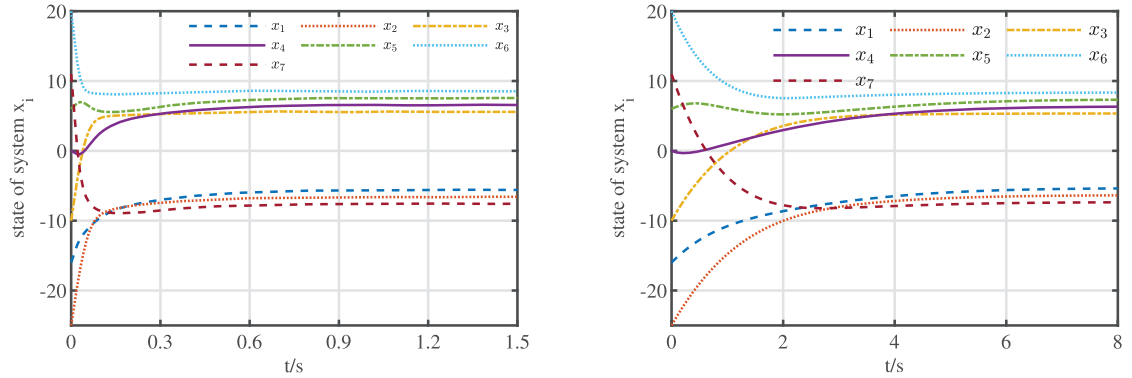

(**a**) The state evolution under $x(0)$ (**b**) The state evolution under $x(0)$ [43]

Figure 5: (Continued)

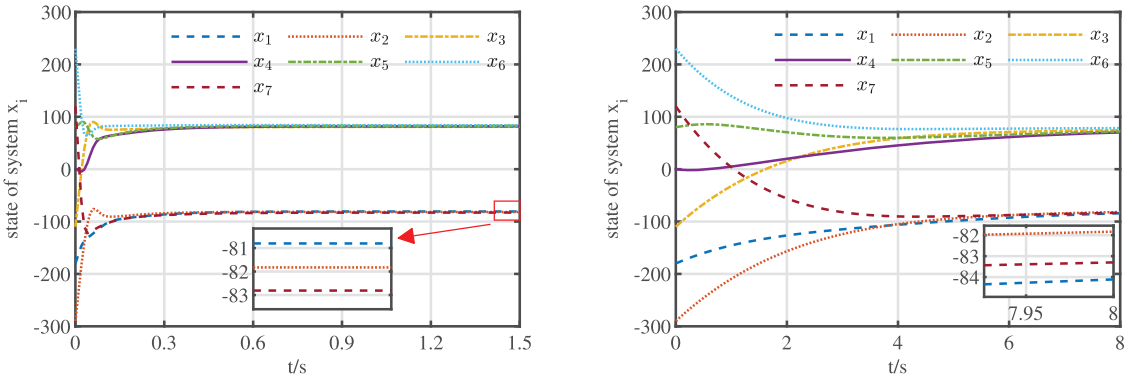

(**c**) The state evolution under $x'(0)$ (**d**) The state evolution under $x'(0)$ [43]

Figure 5: The results of different methods for the controlled multi-agent systems.

4.2 Example 2

Consider a system composed of five unicycle-like nonholonomic robots [45]. The system's communication topology is shown in Fig. 6a, and the schematic diagram of each unicycle-like nonholonomic robot is shown in Fig. 6b. The dynamic model of each robot is given as

$$\begin{cases} \dot{p}_i = v_i \cos \vartheta_i, \\ \dot{q}_i = v_i \sin \vartheta_i, \\ \dot{\vartheta}_i = \varpi_i. \end{cases} \tag{30}$$

where $i = 1, 2, \ldots, 5$, $\Theta_i = [p_i, q_i]^{\mathrm{T}}$ represents the position of robot i in the global coordinate system, ϑ_i represents the orientation of robot i in the coordinate system, v_i is the linear velocity input, and ϖ_i is the angular velocity input. Let the position-like output as $\widehat{\Theta}_i = [\widehat{p}_i, \widehat{q}_i]^{\mathrm{T}}$, with

$$\begin{cases} \widehat{p}_i = p_i + r \cos \vartheta_i, \\ \widehat{q}_i = q_i + r \sin \vartheta_i. \end{cases} \tag{31}$$

where r is a small positive constant.

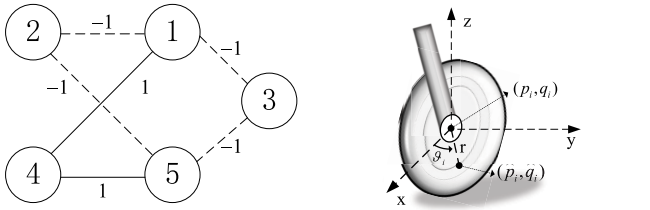

(**a**) Communication topology (**b**) An unicycle-like nonholonomic robot

Figure 6: Unicycle-like nonholonomic robots.

From Eqs. (30) and (31), we have

$$\begin{cases} \dot{\hat{p}}_i = \hat{v}_i, \\ \dot{\hat{q}}_i = \hat{\omega}_i, \\ \dot{\vartheta}_i = \frac{1}{r}(-\hat{v}_i \sin\vartheta_i + \hat{\omega}_i \cos\vartheta_i). \end{cases} \tag{32}$$

where $\hat{v}_i = v_i \cos\vartheta_i - r\omega_i \sin\vartheta_i$ and $\hat{\omega}_i = v_i \sin\vartheta_i + r\omega_i \cos\vartheta_i$ are the virtual inputs for robot i. Since the dynamics of $\hat{p}_i$ and $\hat{q}_i$ have already been transformed into a double-integrator model, we can apply the control methods similar to those in Section 3.

The controller is analogous to Eq. (5).

$$\hat{v}_i(t) = -a_1 P_i^{\mu}(t_k^i) - a_2 P_i^{v}(t_k^i) - a_3 P_i(t_k^i), t \in \left[t_k^i, t_{k+1}^i\right),$$
$$\hat{\omega}_i(t) = -a_1 Q_i^{\mu}(t_k^i) - a_2 Q_i^{v}(t_k^i) - a_3 Q_i(t_k^i), t \in \left[t_k^i, t_{k+1}^i\right).$$

where $P_i(t) = \sum_{j=1}^{N} |a_{ij}| (\hat{p}_i(t) - f_{i1} - sign(a_{ij})(\hat{p}_j(t) - f_{j1}))$ and $Q_i(t) = \sum_{j=1}^{N} |a_{ij}| (\hat{q}_i(t) - f_{i2} - sign(a_{ij})(\hat{q}_j(t) - f_{i2}))$. The dynamic event-triggered conditions are given by Eq. (9).

The initial states of the system are $(p_1, q_1, \vartheta_1) = (2, 3, 0)$, $(p_2, q_2, \vartheta_2) = (-1, 2, \pi)$, $(p_3, q_3, \vartheta_3) = (-3, -1, 0)$, $(p_4, q_4, \vartheta_4) = (4, 4, \pi/2)$, $(p_5, q_5, \vartheta_5) = (0, -1, 0)$, and $\Phi_i(0) = 4$. The desired formation vectors are $f_1 = [1, 2]^{\mathrm{T}}$, $f_2 = [-1, -2]^{\mathrm{T}}$, $f_3 = [-2, -3]^{\mathrm{T}}$, $f_4 = [2, 3]^{\mathrm{T}}$, and $f_5 = [3, 2]^{\mathrm{T}}$. Other parameters are set as $h = 0.01$, $r = 0.5$, $a_1 = 2$, $a_2 = 0.5$, $a_3 = 0.5$, $\mu = 11/9$, $v = 7/9$, $b_1 = 0.3$, $b_2 = 0.1$, $c_1 = 2$, $c_2 = 1$, $\sigma = 0.01$, and $\tau = 10$. The position-like output is shown in Fig. 7a, where $\hat{p}_i$ and $\hat{q}_i$ converge within 0.2 s, exhibiting a fast convergence rate. The dynamic event-triggered intervals are shown in Fig. 7b, which indicates that the designed dynamic event-triggered strategy has a relatively small number of triggers.

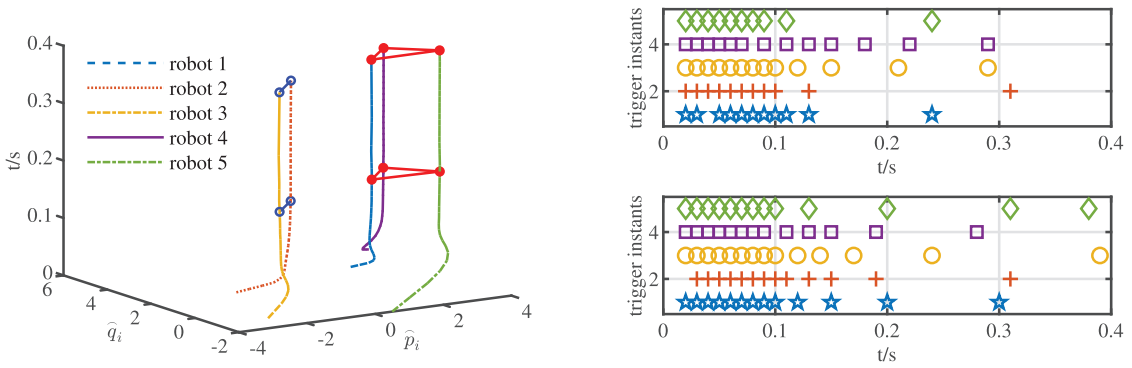

(**a**) The output of position (**b**) The dynamic event-triggered instants

Figure 7: The output and event-triggered instants of the system.

5 Conclusion

This paper proposed a dynamic event-triggered fixed-time bipartite formation control algorithm for continuous-time multi-agent systems with sampled data. First, a periodic sampling mechanism and a dynamic event-triggered communication strategy have been developed. Compared with existing event-triggered methods, our method further reduces communication frequency and avoids the Zeno phenomenon by the designed sampling mechanism. Moreover, cooperative and competitive relationships

among angels have been further considered, and a fixed-time bipartite formation control approach has been developed. In our future efforts, investigating fixed-time bipartite formation control multi-agent systems with non-periodic sampling and without requiring structural balance is meaningful.

Acknowledgement: We would like to express our sincere gratitude to the editors and reviewers for their constructive suggestions, which significantly enhanced the quality of this paper.

Funding Statement: This research was funded in part by the National Natural Science Foundation of China, grant number 62403216, in part by the Basic Research Program of Jiangsu Province, grant number BK20241608, in part by the Jiangsu Province Youth Science and Technology Talent Support Program, grant number JSTJ-2025-544, in part by the Wuxi Young Science and Technology Talent Support Program, grant number TJXD-2024-114, in part by the European Union Intelligent Multi-Agent Robotic Systems (EU iMARs) project, grant number HORIZON-MSCA-2023-101182996, and in part by the 111 project, grant number B23008.

Author Contributions: The authors confirm their contributions to this manuscript as follows: Conceptualization, Longquan Ma and Huarong Zhao; methodology, Linbo Xie and Hongnian Yu; software, Longquan Ma and Liqin Zhou; validation, Longquan Ma, Huarong Zhao, Liqin Zhou, Linbo Xie and Hongnian Yu; formal analysis and investigation, Longquan Ma and Liqin Zhou; resources, Longquan Ma, Huarong Zhao and Linbo Xie; writing—original draft preparation, Longquan Ma and Liqin Zhou; writing—review and editing, Huarong Zhao, Linbo Xie and Hongnian Yu; supervision and project administration, Huarong Zhao and Linbo Xie. All authors reviewed and approved the final version of the manuscript.

Availability of Data and Materials: All reviewed materials are publicly available and cited, primarily sourced from major academic repositories and publishers, including IEEE Xplore, ACM Digital Library, ScienceDirect (Elsevier), SpringerLink, AAAI, Nature, and the arXiv repository.

Ethics Approval: Not applicable.

Conflicts of Interest: The authors declare no conflicts of interest.

References

1. Zhu YM, Kang Z, Zhu HY, Wu S, Zhan X, Shen Q, et al. Robust attitude consensus control of multi-spacecraft with stochastic link failure. Aerosp Syst. 2023;6(4):581–94. doi:10.1007/s42401-023-00204-x.
2. Xie X, Sheng T, Chen X. Self-triggered formation control for multi-spacecraft attitude coordination with communication delays. J Frankl Inst. 2023;360(18):14696–711. doi:10.1016/j.jfranklin.2023.11.021.
3. Quan Y, Xi L. Smart generation system: a decentralized multi-agent control architecture based on improved consensus algorithm for generation command dispatch of sustainable energy systems. Appl Energy. 2024;365:123209.
4. Caicedo AMD, Mejia ÉF, Luna EG. Revolutionizing protection dynamics in microgrids: local validation environment and a novel global management control through multi-agent systems. Comput Electr Eng. 2024;120:109748.
5. Wang J, Luo X, Li M, Guan X. Distributed nonsingular terminal sliding mode control-based RBFNN for heterogeneous vehicular platoons with input saturation. Trans Inst Meas Control. 2024;46(9):1742–54. doi:10.1177/01423312231197848.
6. Iizuka K, Seo T. Passenger-oriented distributed traffic signal control using dynamic programming with vehicle queue spillback and waiting time constraints. Int J Intell Transp Syst Res. 2024;22(3):579–602. doi:10.1007/s13177-024-00418-z.
7. Mohamed H, Marouane H, Fakhfakh A. A systematic review of multi-agent systems and mobile edge computing in intelligent transportation systems. J Soft Comput Data Min. 2025;6(1):169–81. doi:10.30880/jscdm.2025.06.01.012.
8. Farooq A, Xiang Z, Chang WJ, Aslam MS. Recent advancement in formation control of multi-agent systems: a review. Comput Mater Contin. 2025;83(3):1–52. doi:10.32604/cmc.2025.063665.

9. Lin YH, Chang WJ, Lee YC, Aslam MS, Ku CC. Computational design of interval type-2 fuzzy control for formation and containment of multi-agent systems with collision avoidance capability. Comput Model Eng Sci. 2025;144(2):2231–62. doi:10.32604/cmes.2025.067464.
10. Maldonado D, Cruz E, Torres JA, Cruz PJ. Benitez SdPG. Multi-agent systems: a survey about its components, framework and workflow. IEEE Access. 2024;12:80950–75.
11. Chen Y, Zhao H, Ogura M, Yu H, Peng L. Data-driven event-triggered fixed-time load frequency control for multi-area power systems with input delays. IEEE Trans Circuits Syst I Regul Pap. 2025;72(12):8492–504. doi:10.22541/au.172455533.39923476/v1.
12. Zhao H, Shan J, Peng L, Yu H. Learning-based robust bipartite consensus control for a class of multiagent systems. IEEE Trans Ind Electron. 2022;70(4):4068–76. doi:10.1109/tie.2022.3174275.
13. Bu X, Ma W, Yin Y. Event-triggered iterative learning formation control for a class of nonlinear multi-agent systems under deception attack. Asian J Control. 2025;277(11):110797. doi:10.1002/asjc.3675.
14. Olfati-Saber R, Murray RM. Consensus problems in networks of agents with switching topology and time-delays. IEEE Trans Autom Control. 2004;49(9):1520–33. doi:10.1109/tac.2004.834113.
15. Li Z, Tang Y, Huang T, Wen S. Formation control of multiagent networks: cooperative and antagonistic interactions. IEEE Trans Syst Man Cybern Syst. 2021;52(5):2809–18.
16. Ma X, Chou T. Practical time-varying formation cooperative control for high-order nonlinear multi-agent systems avoiding spatial resource conflict via safety constraints. Int J Robust Nonlinear Control. 2024;34(18):11924–52. doi:10.1002/rnc.7600.
17. Li T, Zhao R, Chen CP, Fang L, Liu C. Finite-time formation control of under-actuated ships using nonlinear sliding mode control. IEEE Trans Cybern. 2018;48(11):3243–53. doi:10.1109/TCYB.2018.2794968.
18. Zhang J, Fu Y, Fu J. Adaptive finite-time optimal formation control for second-order nonlinear multiagent systems. IEEE Trans Syst Man Cybern Syst. 2023;53(10):6132–44. doi:10.1109/tsmc.2023.3278262.
19. Zhang J, Tong S. Robust adaptive finite-time containment control for nonlinear multi-agent systems with unknown input saturations. Int J Control. 2024;97(6):1250–61. doi:10.1080/00207179.2023.2204381.
20. Ning B, Han QL, Zuo Z, Ding L, Lu Q, Ge X. Fixed-time and prescribed-time consensus control of multiagent systems and its applications: a survey of recent trends and methodologies. IEEE Trans Ind Inform. 2022;19(2):1121–35.
21. Cheng W, Zhang K, Jiang B, Ding SX. Fixed-time fault-tolerant formation control for heterogeneous multi-agent systems with parameter uncertainties and disturbances. IEEE Trans Circuits Syst I Regul Pap. 2021;68(5):2121–33. doi:10.1109/tcsi.2021.3061386.
22. Zhang J, Fu Y, Fu J. Adaptive fixed-time output-feedback optimal time-varying formation control for multiple omnidirectional robot systems. IEEE Trans Fuzzy Syst. 2024;32(3):792–803. doi:10.1109/tfuzz.2023.3308573.
23. Wang J, Li Y, Wu Y, Liu Z, Chen K, Chen CP. Fixed-time formation control for uncertain nonlinear multi-agent systems with time-varying actuator failures. IEEE Trans Fuzzy Syst. 2024;32(4):1965–77. doi:10.1109/tfuzz.2023.3342282.
24. Zhang Y, Chadli M, Xiang Z. Prescribed-time formation control for a class of multiagent systems via fuzzy reinforcement learning. IEEE Trans Fuzzy Syst. 2023;31(12):4195–204. doi:10.1109/tfuzz.2023.3277480.
25. Zhang Y, Chadli M, Xiang Z. Prescribed-time adaptive fuzzy optimal control for nonlinear systems. IEEE Trans Fuzzy Syst. 2024;32(4):2403–12. doi:10.1109/tfuzz.2024.3352590.
26. Zhang Y, Xiang Z. Prescribed-time optimal control for a class of switched nonlinear systems. IEEE Trans Autom Sci Eng. 2024;22:3033–43. doi:10.1109/tase.2024.3388456.
27. Altafini C. Consensus problems on networks with antagonistic interactions. IEEE Trans Autom Control. 2012;58(4):935–46. doi:10.1109/tac.2012.2224251.
28. Wang W, Huang C, Huang C, Cao J, Lu J, Wang L. Bipartite formation problem of second-order nonlinear multi-agent systems with hybrid impulses. Applied Math Comput. 2020;370(11):124926. doi:10.1016/j.amc.2019.124926.
29. Yang Y, Chen D, Liu Q, Yue D. Predictor-based bipartite time-varying formation control of nonlinear multi-agents systems via disturbance observer. Int J Robust Nonlinear Control. 2022;32(9):5694–716. doi:10.1002/rnc.6114.

30. Ma L, Zhu F. Fixed-time-synchronized bipartite time-varying formation tracking control of networked euler-lagrange systems. IEEE Trans Autom Sci Eng. 2025; 22:3458–69. doi:10.1109/TASE.2024.3395325.
31. Dimarogonas DV, Frazzoli E, Johansson KH. Distributed event-triggered control for multi-agent systems. IEEE Trans Autom Control. 2011;57(5):1291–7. doi:10.1109/tac.2011.2174666.
32. Zhao H, Shan J, Peng L, Yu H. Distributed event-triggered bipartite consensus for multiagent systems against injection attacks. IEEE Trans Ind Inform. 2022;19(4):5377–86. doi:10.1109/tii.2022.3157595.
33. Zhao H, Yu H, Peng L. Event-triggered distributed data-driven iterative learning bipartite formation control for unknown nonlinear multiagent systems. IEEE Trans Neural Netw Learn Syst. 2022;35(1):417–27. doi:10.1109/TNNLS.2022.3174885.
34. Cai Y, Zhang H, Zhang J, Xi R, He Q. Fully distributed bipartite time-varying formation control for uncertain linear multi-agent systems under event-triggered mechanism. Int J Robust Nonlinear Control. 2021;31(11):5165–87. doi:10.1002/rnc.5532.
35. Liu J, Ran G, Wu Y, Xue L, Sun C. Dynamic event-triggered practical fixed-time consensus for nonlinear multiagent systems. IEEE Trans Circuits Syst II Express Briefs. 2021;69(4):2156–60. doi:10.1109/tcsii.2021.3128624.
36. Du X, Qu S, Zhang H, Xu W, Tang Q. Distributed bipartite consensus for multi-agent systems with dynamic event-triggered mechanism. J Frankl Inst. 2023;360(12):8877–97. doi:10.1016/j.jfranklin.2022.05.022.
37. Qi Y, Du C, Zhang X, Mu R. Dynamic event-triggered bipartite consensus for uncertain high-order nonlinear multi-agent systems. Control Theory Technol. 2023;21(2):222–32. doi:10.1007/s11768-022-00121-y.
38. Yazdani S, Haeri M, Su H. Sampled-data leader-follower algorithm for flocking of multi-agent systems. IET Control Theory Appl. 2019;13(5):609–19. doi:10.1109/rios.2017.7956458.
39. Liu W, Huang J. Leader-following consensus for linear multiagent systems via asynchronous sampled-data control. IEEE Trans Autom Control. 2019;65(7):3215–22. doi:10.1109/tac.2019.2948256.
40. Liu H, Wang Z. Sampled-data-based consensus of multi-agent systems under asynchronous denial-of-service attacks. Nonlinear Anal Hybrid Syst. 2021;39(8):100969. doi:10.1016/j.nahs.2020.100969.
41. Peng C, Zhang J, Han QL. Consensus of multiagent systems with nonlinear dynamics using an integrated sampled-data-based event-triggered communication scheme. IEEE Trans Syst Man Cybern Syst. 2018;49(3):589–99. doi:10.1109/tsmc.2018.2814572.
42. Yao Y, Luo Y, Cao J. Finite-time guarantee-cost H∞ consensus control of second-order multi-agent systems based on sampled-data event-triggered mechanisms. Neural Netw. 2024;174(12):106261. doi:10.1016/j.neunet.2024.106261.
43. Yin K, Yang D. Sampled-data-based dynamic event-triggered asynchronous control of continuous-time positive Markov jump systems. Chaos Solitons Fractals. 2023;169(9):113254. doi:10.1016/j.chaos.2023.113254.
44. Parsegov S, Polyakov A, Shcherbakov P. Nonlinear fixed-time control protocol for uniform allocation of agents on a segment. In: Proceedings of the 2012 IEEE 51st IEEE Conference on Decision and Control (CDC); 2012 Dec 10–13; Maui, HI, USA. p. 7732–7.
45. Chen X, Yu H, Hao F. Prescribed-time event-triggered bipartite consensus of multiagent systems. IEEE Trans Cybern. 2020;52(4):2589–98. doi:10.1109/TCYB.2020.3004572.